Published in final edited form as:
J Comp Neurol. 2010 April 15; 518(8): 1330–1348. doi:10.1002/cne.22279.

Quantitative analysis of pre-and postsynaptic sex differences in the nucleus accumbens

Paul M. Forlano[1] and **Catherine S. Woolley**[*]
Department of Neurobiology and Physiology, Northwestern University, Evanston, IL 60208

Abstract

The nucleus accumbens (NAc) plays a central role in motivation and reward. While there is ample evidence for sex differences in addiction-related behaviors, little is known about the neuroanatomical substrates that underlie these sexual dimorphisms. We investigated sex differences in synaptic connectivity of the NAc by evaluating pre- and postsynaptic measures in gonadally intact male and proestrous female rats. We used DiI labeling and confocal microscopy to measure dendritic spine density, spine head size, dendritic length and branching of medium spiny neurons (MSNs) in the NAc, and quantitative immunofluorescence to measure glutamatergic innervation using pre- (vesicular glutamate transporter 1 and 2) and postsynaptic (post synaptic density 95) markers, as well as dopaminergic innervation of the NAc. We also utilized electron microscopy to complement the above measures. Clear but subtle sex differences were identified, namely in distal dendritic spine density and the proportion of large spines on MSNs, both of which are greater in females. Sex differences in spine density and spine head size are evident in both the core and shell subregions, but are stronger in the core. This study is the first demonstration of neuroanatomical sex differences in the NAc and provides evidence that structural differences in synaptic connectivity and glutamatergic input may contribute to behavioral sex differences in reward and addiction.

Keywords

dendritic spines; PSD-95; VGLUT; tyrosine hydroxylase; reward; addiction

The neural circuitry of reward functions to reinforce the acquisition of essential resources for survival and reproduction. Interestingly, both human and animal studies indicate that behavioral responses to rewarding substances differ between males and females (reviewed in Becker and Hu, 2008; Roth et al., 2004; Swendsen et al., 2008). Sex differences are clearest in animal models, particularly with psychostimulants such as cocaine or amphetamine. These studies show that both behavioral sensitization (Hu and Becker, 2003) and the motivation to take drugs, as indicated by conditioned place preference (Russo et al., 2003) or self-administration (Lynch and Carroll, 1999), are greater in female compared to male rats. While it has been hypothesized that estrogen may magnify sex differences in the behavioral response to psychostimulants by affecting sexually dimorphic circuitry (Becker, 1999), the details of the sex differences in the brain's reward circuitry are unknown.

The nucleus accumbens (NAc) is an essential in the neural circuitry of reward, and both dopaminergic and glutamatergic input the NAc are important in the process of addiction. The NAc can be divided into two major subregions, the core and shell, which are

[*]Correspondence to: Catherine S. Woolley, cwoolley@northwestern.edu .
[1]Current address: Department of Biology, Brooklyn College, City University of New York, Brooklyn, NY 11210

distinguished by their chemoarchitecture and function (Di Chiara, 2002; Groenewegen et al., 1999). Ninety percent of neurons in the NAc are γ-aminobutyric acid (GABA)-ergic medium spiny neurons (MSNs), which project to motor regions in the ventral pallidum and ventral mesencephalon. The NAc receives dopamine (DA) projections from the ventral tegmental area (VTA), which also sends afferents to the prefrontal cortex (PFC), ventral subiculum of the hippocampus (VS), and basolateral amygdala (BLA). These nuclei, along with the central thalamic nucleus, in turn provide the major glutamatergic input to the NAc (Kauer and Malenka, 2007; Sesack et al., 2003).

Both dopaminergic and glutamatergic input to the NAc are important in the process of addiction (reviewed in Hyman et al., 2006; Kauer and Malenka, 2007). Glutamatergic synapses on MSNs are formed primarily on dendritic spines, especially in the distal dendrites (Groenewegen et al., 1999). Tract-tracing studies combined with immunocytochemistry for tyrosine hydroxylase (TH) show convergence of DA inputs with glutamatergic afferents from PFC and limbic regions onto dendritic spines of MSNs (Bouyer et al., 1984; Johnson et al., 1994; Sesack and Pickel, 1990; 1992; Totterdell and Smith, 1989; Zahm, 1992). This arrangement of TH-ir and glutamatergic innervation may facilitate DA modulation of glutamate release, and stabilize associated spine synapses (Sesack et al., 2003). Conversely, there is also evidence that dopamine may modulate glutamate release (Gracy and Pickel, 1996). Additionally, several studies have found TH-ir boutons that contain vesicular glutamate transporter 2 (VGLUT2) and/or form excitatory (asymmetric) synapses (Berube-Carriere et al., 2007; Bouyer et al., 1984; Ikemoto et al., 1996; Zahm, 1992), suggesting that some DA neurons may release glutamate.

To investigate potential sexual dimorphisms in the neural circuitry of addiction and reward-related behaviors, we quantified and compared between sexes: 1) morphology of NAc MSN dendrites and dendritic spines visualized with DiI; 2) glutamatergic innervation of the NAc using immunofluorescence for excitatory postsynaptic (PSD-95) and presynaptic (vesicular glutamate transporters, VGLUT1 and 2) markers; 3) immunofluorescence for dopaminergic innervation (TH); and 4) potential DA-glutamate interactions by double-label immunofluorescence for TH and VGLUT2. These light microscopic studies were complemented by characterization of excitatory synapses associated with large spines and TH-ir profiles at the electron microscopic level.

MATERIALS AND METHODS

Animals

Adult male and female Sprague-Dawley rats (Harlan, Indianapolis, IN), 60-67 days old, were used for all experiments. Animals were separated by sex, housed in groups of 2-3 per cage and kept under a 12-hour light:dark cycle. Food and water were available *ad libitum*. Estrous cycles in females were monitored by daily vaginal lavage to confirm normal cycling. Males were handled in parallel, to mitigate any potential differences due to stress. Females were sacrificed on the afternoon of proestrus together with a matched male until a sufficient number of animals for each experiment was accumulated (typically 1 week). All animal procedures were performed in accordance with the National Institutes of Health *Guide for the Care and Use of Laboratory Animals* and were approved by the Northwestern University Institutional Animal Care and Use Committee.

DiI-labeling

Tissue Preparation—Animals (n = 6 males, 6 females) were anesthetized with 80 mg/kg sodium pentobarbital (i.p.) and transcardially perfused with 200 ml of cold, 2% paraformaldehyde in 0.1M phosphate buffer (PB), pH 7.2. Brains were harvested, coded,

and coronal, serial sections were cut with a vibrating tissue slicer (OTS-4000, Electron Microscopy Sciences, Hatfield, PA) in 250 μm thick increments through the NAc (approximately Bregma 2.70 mm to 1.0 mm; Paxinos and Watson, 1998). Slices were stored at 4°C in 0.03% sodium azide in 0.1M PB until fluorescently labeled with DiI (up to approximately one week). The length of storage time did not affect the quality of DiI labeling.

Preparation of "DiOlistic Bullets."—Coating of particles with DiI was adapted from the method described by Gan et al. (2000). Briefly, 5 mg of the carbocyanine fluorescent dye, DiI (Invitrogen, Carlsbad, CA), were dissolved in 130 μl of methylene chloride and allowed to precipitate on 50 mg of tungsten particles (1.3 μm diameter, Bio Rad, Hercules, CA) spread evenly on a glass plate. Particles were dried 5-10 min., scraped off the plate and collected into 3 ml of distilled water. The suspension was briefly vortexed, sonicated for 15 min., and then 0.75 μl PVP solution (20mg/ml polyvinylpropyline in EtOH) was added to minimize clumping of particles. This solution was then resuspended and quickly drawn into nitrogen-dried Tefzel tubing (Bio Rad) and inserted into a tubing prep station (Bio Rad). The tubing was rotated 3-4 times and then particles were allowed precipitate on the tubing wall without rotation for 5 min. The remaining liquid was withdrawn and the tubing was dried for 10 min. under 0.4 LPM nitrogen gas flow. The tubing was then cut into 13 mm segments ("bullets") and stored with desiccant in light-protected and airtight container for up to one month.

Delivery of DiI-Coated Tungsten Particles—A Gene Gun (Bio Rad, Helios Gene Gun System) was powered by helium gas (90-110 psi) for ballistic delivery of coated particles onto tissue sections. Sections were held approximately 2.8 cm from the gun barrel and cell culture inserts (3.0 μm pore-size, Becton Dickinson, Franklin Lakes, NJ) were placed between the tissue and the gun to prevent large clumps of particles from over-labeling brain sections. Labeled tissue was stored in 0.1M PB at 4°C overnight in the dark to allow DiI diffusion throughout cellular membranes. Sections were counterstained with green fluorescent Nissl (1:200 in PB) (Neurotrace, Invitrogen), rinsed in PB and mounted in 2% paraformaldehyde in 0.1M PB in frame-seal chambers. Cells and dendrites were imaged within 7 days of labeling.

Confocal Imaging—A Leica inverted microscope with a spinning disc laser confocal system (PerkinElmer, Wellesley, MA) was used to image three-dimensional dendritic segments with a 100X oil immersion objective by capturing image stacks at 0.2 μm steps in the z plane; whole cells were visualized using a 20X objective to capture image stacks at 0.5 μm steps. Fluorescence emitted by DiI was visualized by excitation with an argon/krypton ion laser (568 nm; CVI Melles Griot, Albuquerque, NM). Nissl counterstain was used under epifluorescence to determine location of labeled structures within the NAc.

Quantification of spine density and spine head size—For the initial spine density analysis, we focused on thin dendrites (0.9-1.2 μm in diameter), characteristic of dendrites distal to the soma (at least secondary or tertiary in branch order), because this is the region of the MSN dendritic tree in which dendritic spine density is most sensitive to psychostimulants (Li et al., 2003; Robinson and Kolb, 1999a). Dendritic spines were analyzed on 10-13 dendritic segments in both the core and shell subregions (21-26 total segments per animal). Confocal image stacks (997 × 635 pixel images, with a pixel size of 0.06 μm in the x and y axes and 0.2 μm in the z axis) were examined using Volocity software (Improvision-PerkinElmer Co., Waltham, MA). Dendritic spines were counted by scrolling through the z plane along approximately 20 μm length of each segment. For branched spines, each termination resulting in a spine head was counted as an individual

spine. Spine number was divided by segment length and spine density was expressed as spines / 10μm.

The same segments of dendrite along which spine density was measured were also evaluated for large (≥ 0.65 μm) and giant (≥ 0.90 μm) diameter spine heads. The diameter of a spine head was measured in the optical section in which it was greatest. From these data, we then calculated large and giant spine density as well as the percentage of large or giant spines along each segment.

Quantification of dendritic arborization—Four to 6 cells were analyzed in both the core and shell subregions (8-11 total per animal). For each whole cell image stack, the length of each dendritic branch was traced in three dimensions using Volocity software and the lengths of all branches were summed for a total dendritic length per cell. Numbers of primary dendrites and terminal dendritic segments per neuron were also calculated. For cells to be included in this analysis, they needed to be unobstructed by adjacent cells or astrocytes and to contain a minimum of 600 μm total dendritic length.

Immunofluorescence

Tissue Preparation—Animals (n = 6 males, 6 females) were deeply anesthetized with 80 mg/kg sodium pentobarbital (i.p.), and transcardially perfused with 4% paraformaldehyde in 0.1M PB. After perfusion, brains were removed and postfixed overnight at 4°C, coded, cryoprotected in 30% sucrose, and cut on a freezing microtome (Leica, Bannockburn, IL) into coronal sections (40μm) spanning the rostrocaudal extent of the NAc. Sections were collected into 4 series and stored in 0.03% sodium azide in 0.1M PB until used for immunohistochemistry.

Immunohistochemistry (IHC)—The 4 series from each animal were used for 1) single labeling with rabbit anti-PSD-95 (1:200; Cell Signaling, Danvers, MA); 2) double-labeling with guinea pig anti-VGLUT1 (1:2000; Millipore, Billerica, MA) and rabbit anti-VGLUT2 (1:1000; Synaptic Systems, Goettingen, Germany); 3) double-labeling with mouse anti-TH (1:1000; Sigma, St. Louis, MO) and rabbit anti-vGLUT2 (1:1000; Synaptic Systems) and 4) controls, including omission of one or both primary antisera, or one or both secondary antibodies. Labeling was absent in all control tissue. Tissue processing was as described previously (Hart et al., 2001; Hart et al., 2007; Ledoux et al., 2009). Briefly, sections were rinsed 2 × 10 min in PB, incubated in 1% sodium borohydride in PB for 10 min, rinsed 3 × 5 min. in PB, 2 × 5 min in 0.1M Tris-buffer pH 7.4 (TB), 3 × 10 min 0.1M Tris-buffered saline (TBS), followed by blocking solution containing 5% normal goat serum (NGS), 3% bovine serum albumin (BSA), 0.3% Triton X-100 in 0.5M TBS for 2 hrs. Sections were incubated in primary antisera diluted in 1% NGS, 2% BSA and 0.3% dimethyl sulfoxide (DMSO) in 0.5M TBS for about 36 hrs at 4°C. Sections were then rinsed 9 × 10 min in 0.1M TBS, and incubated in secondary antibodies (1:800; Invitrogen) for 3 hours at room temperature in the same diluent as primary antisera. Secondary antibodies were: anti-rabbit Alexa Fluor 568 (PSD-95), anti-guinea pig Alexa Fluor 568 (VGLUT1) with anti-rabbit Alexa Fluor 488 (VGLUT2), anti-mouse Alexa Fluor 488 (TH) with anti-rabbit Alexa Fluor 568 (VGLUT2). Sections were then rinsed 3 × 10 min and 3 × 5 min in 0.1M TBS, 1 × 5 min in TB, and 2 × 5 min in PB. Sections were mounted on subbed slides, dehydrated, cleared, rehydrated, and coverslipped under Vectashield (Vector Laboratories, Burlingame, CA).

Antibody characterization—See Table 1 for a list of all antibodies used. The VGLUT1 antibody (Chemicon/ Millipore, # AB5905) detects the expected single ~60kDa band on Western blot (Melone et al., 2005). The double-labeling studies using this and other

VGLUT1 antibodies have demonstrated virtually complete overlap of immunostaining in the rodent brain (Graziano et al., 2008;Melone et al., 2005), and the pattern and type of staining in the striatum is identical to that reported for other VGLUT1 antibodies (e.g., Herzog et al., 2001;Kaneko et al., 2002). Preadsorption with the immunogen peptide (Millipore # AG208) eliminates all staining (manufacturer's technical information).

The VGLUT2 antibody (Synaptic Systems # 135 402) detects a predicted single 65 kDa band on Western blot from brain tissue (Zhou et al., 2007), and no immunostaining is seen when preadsorbed with the immunogen peptide (Synaptic Systems # 135 4P) (Graziano et al., 2008; Zhou et al., 2007). The punctate staining pattern in the striatum and other brain regions is identical to other reports (Flak et al., 2009; Herzog et al., 2001; Kaneko et al., 2002).

The PSD-95 antibody (Cell signaling, # 2507) detects an expected single 95 kDa band on Western blot from rat and mouse brain tissue and preabsorption with the immunogen peptide eliminates all staining (manufacturer's technical information). The staining pattern in rat retina is identical to that seen using a monoclonal PSD-95 antibody made against a different portion of the protein (manufacturer's technical information). The discrete punctate immunofluorescent labeling is consistent with the pattern seen in the brain and spinal cord of other rodent studies that have employed other PSD-95 antibodies (Campos et al., 2008; Henny and Jones, 2006).

The monoclonal (Sigma # T 1299) and rabbit polyclonal (below) (Chemicon/ Millipore, # AB152) TH antisera both recognize a predicted ~60 kDa band on Western blot from rat brain tissue (manufacturer's technical information). Both antibodies label sympathetic neurons (Shi et al., 2008), dopaminergic cell bodies and nerve terminals (manufacturer's technical information), and in this study display identical staining patterns characteristic of dopaminergic terminals in the striatum and NAc seen in other studies (e.g., Kawano et al., 2006).

Imaging and quantification of immunoreactivity—At 3 levels that span the majority of the NAc, (approximately Bregma 1.6, 1.2 and 1.0 mm; (Paxinos and Watson, 1998), confocal images were acquired with a 100X objective in each of 4 shell subregions (vertex, cone, intermediate and ventrolateral) for PSD-95 and VGLUT1/ VGLUT2, or 5 shell subregions for TH/VGLUT2 (above areas plus the arch, since it is a small region that is readily defined by TH-ir; (see Todtenkopf and Stellar, 2000) and 3-4 areas within the core for each hemisphere of each section. Thus, a total of 46 (24 shell, 22 core) or 52 (TH/ VGLUT2 only; 30 shell, 22 core) image stacks were analyzed per brain. Image stacks consisted of 81 μm × 61 μm through 2 μm depth (taken with a z-step of 0.2μm) for a total volume of 9,882 μm^3. Each image stack was analyzed using Volocity software for the number of immunoreactive (-ir) puncta (PSD-95 only; other labeling consisted of varicosities (TH) or appeared clumped and could not be distinguished as discrete units); the average volume per punctum (total –ir volume/puncta number; PSD-95) or total (summed) –ir volume (per 9,882 μm^3; VGLUT1/2 and TH/VGLUT2); average sum intensity per punctum (PSD-95) or total mean intensity (mean –ir intensities of all objects together; VGLUT1 or 2 and TH). Total volume of colocalization of TH-ir and VGLUT2-ir was measured in Volocity, from which the percentage of TH-ir volume colocalized with VGLUT2 was calculated. Data are expressed as mean ± standard error of the mean and comparisons between sexes were made by unpaired, two-tailed *t*-tests with N as the number of animals.

DiI labeling combined with PSD-95 immunofluorescence—Tissue from 2 females was prepared for DiI-labeling (see above) but sectioned at 150 μm. After sections were

labeled with DiI, the above protocol for PSD-95 IHC was followed starting at the first rinses in TB. DMSO was used as a weak detergent in place of Triton-X-100 for the blocking step prior to primary incubation. After secondary labeling (anti-rabbit Alexa Fluor 488), sections were rinsed as above with a final rinse in 0.05M PB, mounted on subbed slides, coverslipped with gelmount (Biomeda, Foster City, CA) and sealed with nail polish. Double-labeled dendritic segments were imaged as above (100 X) with alternating scans using excitation at 568 nm (DiI) and 488 nm (PSD-95) at each step (0.2μm).

Electron microscopy

Methods for tissue preparation for IHC with DAB visualization combined with electron microscopy (EM) were adapted from previously published studies (Cooke and Woolley, 2005b; Hart et al., 2001; Hart et al., 2007). Animals (n = 4 males, 4 females) were deeply anesthetized with 80 mg/kg sodium pentobarbital (i.p.), and transcardially perfused with 2.5% paraformaldehyde/0.5% gluteraldehyde in PB. After perfusion, brains were removed and postfixed overnight at 4°C, cryoprotected with 30% sucrose, and cut on a freezing microtome (Leica) into 2 series of coronal sections (80μm) spanning the rostrocaudal extent of the NAc. One series of sections was immunostained for TH. Sections were incubated in 1% sodium borohydride in PB for 10 min., rinsed and incubated in hydrogen peroxide in 0.1M TB (0.05% for 30 min., 0.10% for 60 min., and 0.05% for 30 min.), rinsed and incubated in blocking solution containing 5% NGS, 3% BSA, 0.3% DMSO in 0.5M TBS for 1 hr. Sections were incubated in rabbit anti-TH (1:2000, Chemicon) diluted in 1% NGS, 2% BSA and 0.3% DMSO in 0.5M TBS for about 36 hrs at 4°C. Sections were then rinsed 9 × 10 min. in 0.1M TBS, and incubated in goat anti-rabbit biotinylated secondary antibody (1:800, Vector Labs) in same diluent as primary antibody for 3 hrs at room temperature. After thorough rinsing, sections were incubated in avidin-biotin horseradish peroxidase (HRP) complex (1:100, Vectastain Elite ABC kit, Vector Labs) for 3 hrs at room temperature. For visualization, tissue was preincubated in diaminobenzidine (DAB; 0.25 mg/ml) dissolved in TB, pH 7.6 for 20 min. Hydrogen peroxide (0.01%) was added to the solution and the reaction continued for 4.5 min until stopped by several rinses in TB. Both series of sections (immunolabeled and not immunolabeled) were then stained with 1% OsO_4, dehydrated in graded ethanols, and flat-embedded in Eponate resin (Ted Pella, Redding, CA). Sections were trimmed to contain the subregion of interest, mounted on BEEM capsules, and coded. A 1 μm semithin section was taken from each block and stained with toluidine blue to identify boundaries of NAc subregions. Single, or short series of 10-12 ultrathin (~80nm) sections were cut using a Reichert Ultracut S ultramicrotome (Leica), collected onto formvar-coated slot grids, stained with 3% uranyl acetate, followed by 2.66% Reynold's lead citrate, and then imaged with a JEOL 1230 transmission electron microscope equipped with a CCD camera. Initially, regions to image (25,000X) were identified by random systematic sampling within NAc subregions and collected in series. A second survey of EM material focused specifically on synapses associated with large dendritic spines and TH-ir profiles and these images were acquired at magnifications up to 40,000X.

Statistical Analysis

For all quantitative analyses, data are expressed as mean ± standard error of the mean and comparisons between sexes were made by unpaired, two-tailed *t*-tests with n as the number of animals.

Image processing

Figures containing confocal images were generated by projecting image stacks onto a single plane in Volocity. All photomicrographs were compiled in Adobe Photoshop and levels

adjusted to enhance contrast when necessary. Line drawings were made in Adobe Illustrator (Adobe Systems, San Jose, CA)

RESULTS

MSN dendritic spine density is sexually dimorphic

We analyzed dendritic spine density on 141 randomly selected DiI-labeled dendritic segments from males (n = 6) and 153 segments from females (n = 6) throughout the rostro-caudal extent of the NAc. These dendrites were further divided into those contained within the core or the shell. Figure 1A shows representative dendritic segments from both the core and shell subregions of males and females used in this study. In the core, spine density ranged from 22-32 spines / 10μm with an average of 26.1 ± 1.5 in females compared to 17-23 spines / 10μm with an average of 21.1 ± 0.9 in males. Females thus have a significantly greater spine density (P = 0.017) in the core, which reflects a 24% sex difference. In the shell, spine density ranged from 19-31 spines / 10μm with an average of 23.4 ± 1.7 in females, compared to 17-23 spines / 10μm with an average of 19.5 ± 0.9 in males. While females were also found to have a greater average spine density in the shell compared to males, the 20% difference was not statistically significant (P = 0.06). However, when data from dendrites in both subregions were combined, females again showed a significantly greater average spine density compared to males (25.0 ± 1.4 vs. 20.4 ± 0.8; P = 0.017), which is a 22% sex difference (Fig. 1B).

No sex difference in MSN dendritic arborization

Several morphological characteristics were measured in DiI-labeled MSNs randomly sampled throughout the NAc (Fig. 2). For both males and females (n = 6), a total of 56 cells were measured: 30 in the core and 26 in the shell. Figure 2A shows a representative DiI-labeled MSN with each dendritic branch color-coded for analyses of: 1) total dendritic length, 2) number of primary dendrites, 3) number of dendritic endings. No rostro-caudal differences in total dendritic length were found within or between sexes, and males and females had virtually the same number of cells in each total dendritic length size class (Fig 2B). We detected no sex differences in any of the morphological parameters examined (Fig. 2C).

One potential concern is that DiI labeling can produce incompletely labeled cells if dendritic segments project out of the plane of section, are too distal from the site of impact of a DiI-coated particle, or are too deep in the tissue and thus too dim for confocal imaging. However, since these caveats apply similarly between animals, and the variability in total dendritic length we measured was equal between sexes, they are unlikely to have obscured a sex difference in MSN dendritic arborization. The lack of sex difference in dendritic arborization, together with the sex difference we observed in dendritic spine density, suggests that the total number of dendritic spines per cell may be greater in females.

Sex difference in PSD-95-ir puncta volume but not density

In order to corroborate dendritic spine density results with an excitatory postsynaptic marker, we quantified the density, volume, and intensity of PSD-95-ir puncta in NAc subregions imaged with confocal microscopy (Fig. 3A). Based on the sex difference in spine density, we expected the density of PSD-95-ir puncta to be greater in females. However, no significant sex differences in the number of PSD-95-ir puncta per image stack were detected in the combined core and shell, the core or shell alone (Fig. 3B), or subregions of the shell (vertex, cone, intermediate and ventrolateral; data not shown) (n = 6; all P values > 0.6).

Females did, however, have a consistently greater average volume and sum intensity of PSD-95-ir puncta in the total NAc and across NAc subregions compared to males. In the shell, the average PSD-95-ir puncta volume was 0.153 ± 0.004 μm^3 in females compared to 0.144 ± 0.001 μm^3 in males (P = 0.037; Fig. 3C). Notably, although non-significant after Bonferroni correction, two subregions of the shell, the ventrolateral (0.157 ± 0.004 μm^3 in females, 0.144 ± 0.004 μm^3 in males; P = 0.045) and cone (0.150 ± 0.005 μm^3 in females compared to 0.140 ± 0.002 μm^3 in males, P = 0.055) regions are the greatest contributors to the shell's overall sex difference. Average puncta volumes in the core were very similar to shell values for both females (0.153 ± 0.005 μm^3) and males (0.145 ± 0.002 μm^3), but variation in the core was slightly greater in each group resulting in no significant sex difference (P = 0.132; Fig. 3C). After combining core and shell data, females again had a greater average but non-significant puncta volume than males (P = 0.07). In a similar pattern, PSD-95-ir puncta sum intensity in the shell was greater in females than males, although the difference was a statistical trend (P = 0.052) (Fig. 3D). Overall, these results indicate that females have, on average, larger and more intensely labeled PSD-95-ir puncta in the NAc compared to males.

The sex difference in dendritic spine density is likely specific for distal dendrites and may not reflect a difference in overall excitatory synapse density in the NAc

We considered several possibilities to explain the discrepancy between a sex difference in dendritic spine density and lack of a sex difference in PSD-95-ir puncta density in the NAc. The PSD-95-ir puncta counted in our confocal images represent a general population of PSDs, and thus include those on distal dendritic spines (where our spine density measurements were made) in addition to proximal dendritic spines, dendritic shafts, and somata of MSNs as well as on the relatively small number of NAc interneurons. First, to investigate PSD-95 at sites other than on dendritic spine heads, we double-labeled tissue for DiI and PSD-95. This revealed many examples of PSD-95-ir puncta on dendritic shafts in addition to spine heads as well as on somata (data not shown) and on thick dendrites proximal to the soma (Fig. 4A, B). Furthermore, our survey of NAc synapses using EM confirmed that excitatory synapses on dendritic shafts were common (Fig. 4C), in accordance with previous reports (French and Totterdell, 2004; Pinto et al., 2003; Smith and Bolam, 1990). Thus, only a portion of PSD-95-ir puncta and excitatory synapses in the NAc are found on dendritic spine heads.

It is also possible that the sex difference in MSN dendritic spine density is restricted to distal dendrites. Synapses on proximal spines or dendritic shafts might have obscured such a difference in the PSD-95 analysis. To test this idea, we returned to our confocal image stacks of DiI labeled dendrites and measured spine density specifically on thick (> 1.2 μm) dendritic segments, which presumably are more proximal than the thinner segments. We compared spine density on 24 thick segments throughout the NAc of females (n = 6) and 16 thick segments in males (n = 5). As expected, spine densities were greater on thick dendrites compared to our previous analysis of thin dendrites: 30.0 ± 2.7 in females and 28.4 ± 2.8 spines / 10μm in males (P = 0.7; Fig. 4D). Thus, although the sample size was limited, there is no trend toward females having greater spine density in thicker, likely proximal, dendritic segments. These results support the idea that dendritic spine density on MSNs is sexually dimorphic specifically within the distal portion of the dendritic tree. Together with our analysis of PSD-95-ir, these findings indicate that excitatory synaptic input at sites other than distal dendritic spines may not be sexually dimorphic, resulting in no sex difference in overall excitatory synapse density in the NAc.

Sex differences in spine head size

We also pursued the second unexpected finding from the PSD-95 analysis, a trend toward greater PSD-95-ir puncta volume in females, which could be related to a difference in spine head size. We used the same dendritic segments as in our initial spine density analysis (Fig. 1) to quantify the numbers of "large" (≥ 0.65 μm) and "giant" (≥ 0.9 μm) diameter spine heads (Fig. 5A). Consistent with PSD-95-ir results, we found that females have a significantly greater density of large spines than males in the core (3.9 ± 0.3 vs. 2.6 ± 0.1 spines / 10 μm; P = 0.013), shell (3.8 ± 0.2 vs. 2.8 ± 0.2 spines / 10 μm; P = 0.015), and both subregions combined (3.8 ± 0.2 vs. 2.6 ± 0.1 spines / 10 μm; P = 0.0003) (Fig. 5B), which reflect 51%, 34% and 45 % sex differences, respectively. Females also had a 37% greater density of giant spines compared to males, considering the core and shell combined (1.3 ± 0.1 vs. 0.9 ± 0.1 spines/ 10 μm; P = 0.03) (Fig. 5C). Giant spine densities in females also were also greater in the core and shell separately, but these differences were not statistically significant.

To confirm that the sex differences in large and giant spine density were not simply due to greater spine density in females, we calculated the percentage of all spines that fell into each size category. This revealed that females have a greater percentage of large spines (16.2% ± 0.6% vs. 13.5% ± 0.2%; P = 0.007) (Fig. 5D), though there was no significant sex difference in percentage of giant spines (Fig. 5E). Interestingly, there was no relationship between spine density and percent large or giant spines in either sex or in any subregion (e.g., R^2 = 0.43, P = 0.16 for females large spines; R^2 = 0.1, P = 0.54 for female giant spines for both subregions combined), and even in the cases where individual female and male spine densities overlapped, females had a greater percentage of large spines. Thus, both DiI and PSD-95-ir analyses show that females have more dendritic spines with large heads than males do, which could be related to a sex difference in synaptic strength.

Ultrastructural features of large spine heads

To gain more insight into large and giant dendritic spines, we surveyed NAc synapses at the electron microscopic level. Figure 6 shows several examples of synapses on large and giant spine heads. Synapses on spines invariably included an asymmetric PSD, characteristic of an excitatory synapse. Furthermore, most single sections of large/giant spines and all large/giant spines contained within serial sections had a distinguishable perforation in the PSD (Figs. 6A1, B1, B3, C-E). Spine heads with diameters of at least 1 μm were often observed and some spines had head diameters of up to 2 μm. These spines, which correspond to the giant spines identified in our DiI analysis, invariably contained clumps of vesicles that resemble recycling endosomes (Fig. 6A2) (Park et al., 2006), and often a spine apparatus (Fig. 6B, C). Some of the largest spine heads were "goblet-like" and partially enveloped their associated excitatory bouton (Fig. 6D). Occasionally, giant spines contained a mitochondrion (Fig. 6C). In some cases, the bouton contacting a large/giant spine head also formed a second synapse, typically with a much smaller spine (Fig. 6A).

Vesicular glutamate transporter1 and 2-ir vary among NAc subregions but are not sexually dimorphic

To complement analysis of excitatory postsynaptic measures, we also evaluated the two most prevalent excitatory presynaptic markers in the NAc, VGLUT1 and VGLUT2, in the core and subregions of the shell in alternate sections from the same animals used for the PSD-95 study. VGLUT1 and VGLUT2 labeling was very dense and varicose (Fig. 7A, B), which precluded analysis of individual labeled puncta as we did for PSD-95. Instead, we quantified VGLUT1 and VGLUT 2-ir volume density and mean intensity per image stack. As others have reported (Herzog et al., 2001), there was little to no colocalization of VGLUT1 and VGLUT2, and the two markers were differentially distributed throughout the

NAc subregions (Fig. 7C, D). There were no sex differences in either VGLUT1 or VGLUT2, so data from males and females were combined. In both sexes, the volume density (μm^3 / stack) of VGLUT1-ir was greatest in the core (740 ± 64) and ventrolateral shell (741 ± 67) and lower in the dorsomedial shell, which includes the vertex (602 ± 77), cone (512 ± 109) and intermediate zone (573 ± 73). In contrast, VGLUT2-ir was highest in the dorsomedial shell: vertex (1051 ± 53), cone (1091 ± 45) and intermediate zone (857 ± 56) and lowest in the ventrolateral shell (630 ± 48) and core (564 ± 50) (Fig. 7C). Thus, the ratio of VGLUT1:VGLUT2 -ir volume is highly complementary among the NAc subregions. Variation in the mean intensity of VGLUT1-ir among NAc subregions paralleled that of VGLUT1-ir volume, whereas the mean intensity of VGLUT2-ir was similar across the core and dorsomedial shell and lowest in the ventrolateral subregion (Fig. 7D). These results demonstrate that, in contrast to postsynaptic markers in the NAc, presynaptic glutamatergic markers show considerable variation across subregions but are not sexually dimorphic.

Tyrosine hydroxylase-ir varies among NAc subregions but is not sexually dimorphic

To investigate sex differences in dopaminergic innervation throughout the core and subregions of the shell, we quantified tyrosine hydroxylase (TH) -ir in alternate sections from the same animals used for PSD-95 and VGLUT1, 2. As expected, TH-ir was characterized by fibers with highly variable varicosities (Fig. 8A), and thus, like VGLUT-ir, TH-ir was quantified on the basis of–ir volume density and mean intensity per image stack. We sampled the same subregions of the shell as above with the additional subregion of the arch, which is not readily discernable without TH labeling. Our quantitative measurements are consistent with previous studies (Todtenkopf and Stellar, 2000) that show high variation in TH-ir labeling across shell subregions, with an alternating pattern of high (vertex, cone, ventrolateral) and medium (arch, intermediate) levels of label; labeling was lightest in the core (Fig. 8D). As for VGLUT1 and 2, TH-ir was not sexually dimorphic so data from males and females were combined. As expected, TH-ir volume / image stack was higher in the shell (437 ± 39) compared to the core (318 ± 35). Within the shell, the cone had the highest TH-ir volume/ stack (585 ± 53) and the arch the lowest (352 ± 38) (Fig. 8D).

Because VGLUT2 was previously demonstrated in a subpopulation of TH-ir terminals in the NAc (Descarries et al., 2008) we quantified percent of TH-ir colocalized with VGLUT2-ir per image stack among NAc subregions (Fig. 8A-D) and compared these values between sexes. Both males and females showed a similar pattern in percent volume of TH-ir colocalized with VGLUT2-ir across NAc subregions, with dorsomedial shell (vertex, arch, cone) > intermediate > core and ventrolateral shell (Fig. 8D). The percent volume of TH-ir colocalized with VGLUT2-ir was essentially the same between sexes in the core (3.3 ± 0.3% in females vs. 3.5 ± 0.1% in males) and slightly higher in females throughout the shell (5.4 ± 0.6% vs. 4.5 ± 0.3%; $P = 0.21$), notably in the dorsomedial shell (6.3 ± 0.6% vs. 4.9 ± 0.5%; $P = 0.10$) which includes the cone (6.6 ± 0.7% vs. 4.9 ± 0.5%; $P = 0.08$) subregion. Thus the highest percentage of TH-ir colocalized with VGLUT2-ir was found in the dorsomedial shell and suggests this is the most likely region where co-release of dopamine and glutamate may occur.

We processed TH-immunolabeled tissue for EM in order to characterize types of TH-ir profiles associated with excitatory synapses in the NAc. As expected, TH-ir was concentrated throughout axons and varicosities (Fig. 8E). Our survey of TH-ir profiles in the NAc is consistent with other studies (Bouyer et al., 1984;Meredith, 1999;Sesack et al., 2003;Voorn et al., 1986;Zahm, 1992) where TH-ir varicosities converge on spines also containing an asymmetric, presumably excitatory, synapse (Fig. 8F, G). Less frequently, a small amount of TH-ir was found in axonal boutons that formed an excitatory synapse with a spine head. In these cases, TH-ir could be either proximal (Fig. 8H) or distal (Fig. 8I) to

the synapse. These findings, along with our confocal data, provide further evidence that a small percentage of boutons in the NAc may co-release glutamate and DA.

DISCUSSION

The behavioral effects of psychostimulants differ between males and females, and in general, females are more responsive (reviewed in Becker and Hu, 2008; Festa et al., 2004; Quinones-Jenab, 2006). The simplest idea to explain these behavioral sex differences is that the neural substrate on which psychostimulants act is sexually dimorphic. We tested this in rats by evaluating pre- and postsynaptic measures in the NAc of gonadally intact males and proestrous females. We found that there are some clear sex differences, but they are subtle. The biggest differences are in distal dendritic spine density and the proportion of large spines on MSNs, both of which are greater in females. Sex differences in spine density and spine size are evident in both the core and shell subregions, but are stronger in the core.

Sex difference in spine density

The sex difference in spine density we report here supports the idea that females have more glutamatergic input onto the distal dendrites of MSNs. Interestingly, it is also the distal region of MSN dendrites where spine density and the number of branched spines increase after a variety of drug treatments (Brown and Kolb, 2001; Robinson and Kolb, 1997; 1999a; b); proximal dendritic branches do not show this plasticity (Li et al., 2003). This is potentially significant because the proximal and distal regions of MSN dendrites receive differential input, especially in the core where the sex difference in spine density is most pronounced.

The core of the NAc is functionally and anatomically more like the dorsal striatum than the NAc shell (Groenewegen et al., 1999; Kelley, 1999; Zahm, 1999; Zahm and Brog, 1992), and there are notable differences in synaptic connectivity of the core and shell. In both the NAc core and dorsal striatum, the majority of extrinsic inputs innervate distal dendrites and spines, and inputs from local circuit neurons (choline actyltransferase, somatostatin, calretinin, enkephalin, dynorphin, and substance P) predominate on proximal dendrites and spines (Groenewegen et al., 1999; Meredith, 1999; Meredith and Totterdell, 1999; Sesack et al., 2003; Smith and Bolam, 1990). In contrast, intrinsic and extrinsic inputs in the caudal medial shell (where most data on shell connectivity have been acquired) are more dispersed among distal and proximal dendrites (French and Totterdell, 2002; 2003; Meredith, 1999; Meredith and Totterdell, 1999; Mulder et al., 1998). In accordance with our findings, others have reported that shell neurons are, on average, less spiny than core neurons (Meredith et al., 1992). Putting these results together, higher spine density, as well as the more robust sex difference in spine density, in the core may be related to the comparatively greater density of glutamatergic input to distal dendrites in this region. From what is known about the innervation patterns of afferents to the NAc, prefrontal cortical (PFC) projections may contribute most to the sex difference in distal spine density in the core, as distal spines in that area invariably receive input from the PFC (Sesack and Pickel, 1992; Smith and Bolam, 1990; Somogyi et al., 1981).

The core and shell also contain differential dopaminergic input. For instance, in the core, TH-ir terminals contact distal spine necks and dendrites, whereas TH-ir terminals in the caudal medial shell are found preferentially on proximal dendritic shafts (Meredith et al., 1993; Totterdell and Smith, 1989; Zahm, 1992). Thus, dopamine-glutamate interactions on spines (i.e., “triad” arrangement) in the shell are reduced compared to those in the core (Meredith and Totterdell, 1999). Since spine density on NAc MSNs is positively regulated by DA (Meredith et al., 1995), lower spine density in males may indicate that males have fewer DA inputs convergent on distal dendrites than females. Taken together, sex

differences in the density of glutamatergic inputs and their interaction with DA in the distal part of MSN dendrites in the core are likely to be important in behavioral sex differences in response to psychostimulants, such as locomotor activity, which is attributed largely to function of the NAc core (David et al., 2004; Kelley, 1999).

It is also possible that sex differences in circulating estradiol contribute to the sex difference in spine density in the NAc, as estradiol is a well documented regulator of spine plasticity in other brain areas (e.g., Calizo and Flanagan-Cato, 2000; Hao et al. 2006; Woolley and McEwen, 1992) (reviewed in Cooke and Woolley, 2005a). However, very few nuclear estrogen receptors (ERs) are reported in the core (ERβ-ir) and none are found in the shell (Shughrue and Merchenthaler, 2001). An estradiol-dependent sex difference in spine density could be established independently of classical ERs, as demonstrated in the developing hypothalamus, where estradiol induces a rapid increase in presynaptic glutamate release that subsequently increases dendritic spine formation (Schwarz et al., 2008). Whether estradiol has direct or indirect effects on spine density in the NAc will be an important topic for future investigations.

Sex difference in spine head size

The values we obtained for spine density and spine head size in the NAc are consistent with a recent study using similar labeling methods (Shen et al., 2008). In the present study, we found that females have more large spines, over and above their greater overall spine density. Furthermore, there was no correlation between spine density and percent of large spines, also consistent with Shen et al. (2008). Thus, in general, greater spine density does not predict a greater percentage of any one spine type (e.g., small or large). Additionally, our ultrastructual description of large spines in the NAc showed similar features as have been reported for large spines in other brain areas, specifically that large spines contain a perforated PSD, clumps of recycling endosomes/vesicles, and sometimes a spine apparatus.

Large variability in spine size suggests that the functional properties of spines are also highly variable, and that synaptic strength may vary widely among spines along the same dendrite (Arellano et al., 2007). As noted above, large spines typically have large perforated PSDs (reviewed in Arellano et al., 2007; Bourne and Harris, 2008). In other brain regions, large perforated PSDs contain an especially high density of AMPARs (e.g., Ganeshina et al., 2004; Matsuzaki et al., 2001; reviewed in Spruston, 2008), predicting greater synaptic strength. Thus, the greater spine head size and PSD-95-ir volume that we found in females, combined with females' greater overall spine density, suggests that MSNs in females have more strong excitatory synapses compared to males.

This sex difference in spine size may also indicate a difference in synaptic plasticity. For example, many studies have demonstrated that LTP induction increases spine head size (e.g., Desmond and Levy, 1983; Matsuzaki et al., 2004), the frequency of perforated PSDs (Geinisman, 2000; Popov et al., 2004), and draws recycling endosomes, vesicular clumps, and polyribosomes from the dendritic shaft into spines (Bourne et al., 2007; Ostroff et al., 2002; Park et al., 2006). These changes occur in parallel with increasing synaptic strength, in part though the incorporation of additional AMPARs into synapses. Therefore, it is possible that the greater number of large spines in females reflects a history of activity-dependent plasticity at more of their synapses.

Another, not mutually exclusive, possibility is that the greater proportion of large spines in females is related to differential synaptic input. For example, a study by French and Totterdell (2004) quantified morphological differences in synapses made by the major glutamatergic afferents to the NAc: PFC, ventral subiculum (VS), basolateral amygdala (BLA), and central medial thalamus (CMT). Afferents from the VS contained the largest

average bouton area, followed by CMT; VS afferents also had significantly larger postsynaptic target areas (spines and shafts) than all other afferents, while the PFC contained the smallest target areas (likely small spines). Based on these data, large spines in the NAc have the highest probability of being contacted by afferents from the VS, followed by the CMT, while small spines are more likely contacted by PFC afferents. Pinto et al. (2003) also noted some large spines with perforated PSDs in the shell that were specifically contacted by thalamic afferents. Similarly, in the lateral amygdala, thalamic and cortical afferents preferentially synapse on large and small spines, respectively (Humeau et al., 2005). Thus, the sex difference in spine head size in the NAc may be related to females having relatively more input from the VS and thalamus.

No sex differences in TH and VGLUT labeling

Glutamatergic terminals from the PFC, BLA and VS are thought to express VGLUT1 exclusively, while terminals from the thalamus express VGLUT2 as well as VGLUT1 (Herzog et al., 2001). Although we found no sex differences in overall glutamatergic input to the NAc, our subregional analysis of presynaptic markers highlights the heterogeneity of glutamatergic inputs throughout the NAc. For example, the high ratio of VGLUT2:VGLUT1 we observed in the dorsomedial shell supports other evidence for robust projections of the thalamus to this portion of the shell (Berendse and Groenewegen, 1990; Pinto et al., 2003). Despite the lack of sex differences in our study, it is possible that proportion of terminals from specific glutamatergic afferents differs between males and females, as suggested above. Tract tracing or cell type-specific markers would be required to investigate this further.

Similar to the analysis of glutamatergic input, our quantification of TH-ir in the core and 5 subregions of the shell revealed no sex differences. Consistent with previous studies (Todtenkopf and Stellar, 2000), however, we found high variation in TH-ir with an alternating pattern of high (vertex, cone, ventrolateral) and medium (arch, intermediate) labeling in the shell, and consistently lower labeling throughout the core. The lack of sex difference in TH-ir was somewhat surprising, given well-documented sex differences in basal and evoked DA release in the striatum, since similar mechanisms are thought to operate in the NAc (see below; Becker and Hu, 2008; Walker et al., 2000).

Other possibilities for sex differences in reward circuitry

It is unlikely the robust behavioral sex differences in response to psychostimulants can be fully explained by the morphological sex differences in the NAc we report here. Given the subtlety of structural sex differences in the NAc, it seems likely that differences in the way NAc (and other) neurons respond to psychostimulants contribute to sex differences in behavior and DA release, perhaps in synergy with differences in structural wiring of the NAc. Interestingly, a recent study found that females have a significantly greater proportion of midbrain dopaminergic neurons that project to the PFC compared to males (Kritzer and Creutz, 2008). Therefore, it is possible that some sex differences arise from differential DA modulation of PFC input to the NAc in females compared to males.

Becker and colleagues have demonstrated robust, estradiol-dependent sex differences in DA release and drug-induced locomotor behavior (reviewed in Becker, 1999; Becker and Hu, 2008). Interestingly, neither estradiol nor castration affects DA release or psychostimulant-induced behavior in males (Becker, 1990; Castner et al., 1993), demonstrating sex-specificity of estradiol's effects. Therefore, in females, estradiol may modulate the function of relevant neural circuits, such as by influencing the excitability of DA neurons in the VTA (Zhang et al., 2008). Additionally, ERs expressed in afferents to the NAc (VTA, VS, BLA, CMT, PFC) may contribute to estradiol's effects on psychomotor behaviors, and/or

indirectly affect NAc MSN structure and function. While the amygdala is replete with both ERα and ERβ-ir neurons, VS, PFC and to a lesser degree CMT, contain some ERβ-ir but virtually no ERα-ir neurons (Shughrue and Merchenthaler, 2001). Nuclear ERβ-ir is found in the VTA but not in afferents that project to the NAc (Creutz and Kritzer, 2004).

It is also important to note that effects of estradiol on drug-induced behavior and DA release in the NAc and striatum can occur in a "rapid" non-genomic fashion (Becker, 1999; Becker and Hu, 2008; Thompson and Moss, 1994), possibly through a G-protein-coupled membrane ER (Mermelstein et al., 1996); also see (Mermelstein, 2009) for review of related non-genomic signaling). There is also evidence that estradiol increases DA release in the striatum by rapid inhibition of intrinsic GABA neurons through membrane-associated ERα, disinhibiting DA release from nearby terminals (Hu et al., 2006; Schultz et al., 2009). In the NAc, several pharmacological studies suggest that ERβ is important in estradiol's effects on drug-induced behavior and DA receptor upregulation (Le Saux et al., 2006; Silverman and Koenig, 2007). Localization of ERs at the subcellular level in the NAc is unexplored and would illuminate potential sites of non-genomic estradiol action.

Conclusions

While estradiol enhances behavioral sensitization and drug acquisition in females, sex differences are still apparent when animals are deprived of gonadal hormones by ovariectomy or castration (reviewed in Becker and Hu, 2008; Festa et al., 2004; Quinones-Jenab, 2006). Our findings are the first to demonstrate a neuroanatomical substrate in the NAc that may contribute to behavioral sex differences in reward and addiction. These structural sex differences are evident in the density and size of dendritic spines in the distal dendrites of MSNs, the major sites of glutamatergic and dopaminergic convergence, particularly in the core. Thus, sex differences in glutamatergic innervation in combination with hormonal modulation of DA release in the NAc and other nuclei may act in a synergistic fashion to produce sex differences in reward-related behaviors.

Supplementary Material

Refer to Web version on PubMed Central for supplementary material.

Acknowledgments

We thank Andrew McCollum, Surina Kumar and Lidia Spaho for quantitative assistance and Renee May, Melissa Snyder and Brad Cooke for technical advice.

Grant sponsor: National Institutes of Health F32 DA 025449 (P.M.F.) and R01 DA 020492 (C.S.W.)

LITERATURE CITED

Arellano JI, Benavides-Piccione R, Defelipe J, Yuste R. Ultrastructure of dendritic spines: correlation between synaptic and spine morphologies. Front Neurosci. 2007; 1:131–143. [PubMed: 18982124]

Becker JB. Direct effect of 17 beta-estradiol on striatum: sex differences in dopamine release. Synapse. 1990; 5:157–164. [PubMed: 2309159]

Becker JB. Gender differences in dopaminergic function in striatum and nucleus accumbens. Pharmacol Biochem Behav. 1999; 64:803–812. [PubMed: 10593204]

Becker JB, Hu M. Sex differences in drug abuse. Front Neuroendocrinol. 2008; 29:36–47. [PubMed: 17904621]

Berendse HW, Groenewegen HJ. Organization of the thalamostriatal projections in the rat, with special emphasis on the ventral striatum. J Comp Neurol. 1990; 299:187–228. [PubMed: 2172326]

Berube-Carriere N, Riad M, Dal Bo G, Trudeau L-E, Descarries L. Vesicular glutamate transporter 2 in dopamine axon terminals of the nucleus accumbens. Society for Neuroscience Abstracts. 2007; 38:9.

Bourne JN, Harris KM. Balancing structure and function at hippocampal dendritic spines. Annu Rev Neurosci. 2008; 31:47–67. [PubMed: 18284372]

Bourne JN, Sorra KE, Hurlburt J, Harris KM. Polyribosomes are increased in spines of CA1 dendrites 2 h after the induction of LTP in mature rat hippocampal slices. Hippocampus. 2007; 17:1–4. [PubMed: 17094086]

Bouyer JJ, Joh TH, Pickel VM. Ultrastructural localization of tyrosine hydroxylase in rat nucleus accumbens. J Comp Neurol. 1984; 227:92–103. [PubMed: 6147361]

Brown RW, Kolb B. Nicotine sensitization increases dendritic length and spine density in the nucleus accumbens and cingulate cortex. Brain Res. 2001; 899:94–100. [PubMed: 11311869]

Calizo LH, Flanagan-Cato LM. Estrogen selectively regulates spine density within the dendritic arbor of rat ventromedial hypothalamic neurons. J Neurosci. 2000; 20:1589–1596. [PubMed: 10662848]

Campos LW, Chakrabarty S, Haque R, Martin JH. Regenerating motor bridge axons refine connections and synapse on lumbar motoneurons to bypass chronic spinal cord injury. J Comp Neurol. 2008; 506:838–850. [PubMed: 18076081]

Castner SA, Xiao L, Becker JB. Sex differences in striatal dopamine: in vivo microdialysis and behavioral studies. Brain Res. 1993; 610:127–134. [PubMed: 8518920]

Cooke BM, Woolley CS. Gonadal hormone modulation of dendrites in the mammalian CNS. J Neurobiol. 2005a; 64:34–46. [PubMed: 15884004]

Cooke BM, Woolley CS. Sexually dimorphic synaptic organization of the medial amygdala. J Neurosci. 2005b; 25:10759–10767. [PubMed: 16291949]

Creutz LM, Kritzer MF. Mesostriatal and mesolimbic projections of midbrain neurons immunoreactive for estrogen receptor beta or androgen receptors in rats. J Comp Neurol. 2004; 476:348–362. [PubMed: 15282710]

David HN, Sissaoui K, Abraini JH. Modulation of the locomotor responses induced by D1-like and D2-like dopamine receptor agonists and D-amphetamine by NMDA and non-NMDA glutamate receptor agonists and antagonists in the core of the rat nucleus accumbens. Neuropharmacology. 2004; 46:179–191. [PubMed: 14680757]

Descarries L, Berube-Carriere N, Riad M, Bo GD, Mendez JA, Trudeau LE. Glutamate in dopamine neurons: synaptic versus diffuse transmission. Brain Res Rev. 2008; 58:290–302. [PubMed: 18042492]

Desmond NL, Levy WB. Synaptic correlates of associative potentiation/depression: an ultrastructural study in the hippocampus. Brain Res. 1983; 265:21–30. [PubMed: 6850319]

Di Chiara G. Nucleus accumbens shell and core dopamine: differential role in behavior and addiction. Behav Brain Res. 2002; 137:75–114. [PubMed: 12445717]

Festa ED, Russo SJ, Gazi FM, Niyomchai T, Kemen LM, Lin SN, Foltz R, Jenab S, Quinones-Jenab V. Sex differences in cocaine-induced behavioral responses, pharmacokinetics, and monoamine levels. Neuropharmacology. 2004; 46:672–687. [PubMed: 14996545]

Flak JN, Ostrander MM, Tasker JG, Herman JP. Chronic stress-induced neurotransmitter plasticity in the PVN. J Comp Neurol. 2009; 517:156–165. [PubMed: 19731312]

French SJ, Totterdell S. Hippocampal and prefrontal cortical inputs monosynaptically converge with individual projection neurons of the nucleus accumbens. J Comp Neurol. 2002; 446:151–165. [PubMed: 11932933]

French SJ, Totterdell S. Individual nucleus accumbens-projection neurons receive both basolateral amygdala and ventral subicular afferents in rats. Neuroscience. 2003; 119:19–31. [PubMed: 12763065]

French SJ, Totterdell S. Quantification of morphological differences in boutons from different afferent populations to the nucleus accumbens. Brain Res. 2004; 1007:167–177. [PubMed: 15064148]

Ganeshina O, Berry RW, Petralia RS, Nicholson DA, Geinisman Y. Synapses with a segmented, completely partitioned postsynaptic density express more AMPA receptors than other axospinous synaptic junctions. Neuroscience. 2004; 125:615–623. [PubMed: 15099675]

Geinisman Y. Structural synaptic modifications associated with hippocampal LTP and behavioral learning. Cereb Cortex. 2000; 10:952–962. [PubMed: 11007546]

Gracy KN, Pickel VM. Ultrastructural immunocytochemical localization of the N-methyl-D-aspartate receptor and tyrosine hydroxylase in the shell of the rat nucleus accumbens. Brain Res. 1996; 739:169–181. [PubMed: 8955937]

Graziano A, Liu XB, Murray KD, Jones EG. Vesicular glutamate transporters define two sets of glutamatergic afferents to the somatosensory thalamus and two thalamocortical projections in the mouse. J Comp Neurol. 2008; 507:1258–1276. [PubMed: 18181146]

Groenewegen HJ, Wright CI, Beijer AV, Voorn P. Convergence and segregation of ventral striatal inputs and outputs. Ann N Y Acad Sci. 1999; 877:49–63. [PubMed: 10415642]

Hao J, Rapp PR, Leffler AE, Leffler SR, Janssen WG, Lou W, McKay H, Roberts JA, Wearne SL, Hof PR, Morrison JH. Estrogen alters spine number and morphology in prefrontal cortex of aged female rhesus monkeys. J Neurosci. 2006; 26:2571–2578. [PubMed: 16510735]

Hart SA, Patton JD, Woolley CS. Quantitative analysis of ER alpha and GAD colocalization in the hippocampus of the adult female rat. J Comp Neurol. 2001; 440:144–155. [PubMed: 11745614]

Hart SA, Snyder MA, Smejkalova T, Woolley CS. Estrogen mobilizes a subset of estrogen receptor-alpha-immunoreactive vesicles in inhibitory presynaptic boutons in hippocampal CA1. J Neurosci. 2007; 27:2102–2111. [PubMed: 17314305]

Henny P, Jones BE. Innervation of orexin/hypocretin neurons by GABAergic, glutamatergic or cholinergic basal forebrain terminals evidenced by immunostaining for presynaptic vesicular transporter and postsynaptic scaffolding proteins. J Comp Neurol. 2006; 499:645–661. [PubMed: 17029265]

Herzog E, Bellenchi GC, Gras C, Bernard V, Ravassard P, Bedet C, Gasnier B, Giros B, El Mestikawy S. The existence of a second vesicular glutamate transporter specifies subpopulations of glutamatergic neurons. J Neurosci. 2001; 21:RC181. [PubMed: 11698619]

Hu M, Watson CJ, Kennedy RT, Becker JB. Estradiol attenuates the K+-induced increase in extracellular GABA in rat striatum. Synapse. 2006; 59:122–124. [PubMed: 16320305]

Humeau Y, Herry C, Kemp N, Shaban H, Fourcaudot E, Bissiere S, Luthi A. Dendritic spine heterogeneity determines afferent-specific Hebbian plasticity in the amygdala. Neuron. 2005; 45:119–131. [PubMed: 15629707]

Ikemoto K, Satoh K, Kitahama K, Maeda T. Demonstration of a new dopamine-containing cell group in the primate rostral telencephalon. Neurosci Lett. 1996; 220:69–71. [PubMed: 8977151]

Johnson LR, Aylward RL, Hussain Z, Totterdell S. Input from the amygdala to the rat nucleus accumbens: its relationship with tyrosine hydroxylase immunoreactivity and identified neurons. Neuroscience. 1994; 61:851–865. [PubMed: 7530817]

Kaneko T, Fujiyama F, Hioki H. Immunohistochemical localization of candidates for vesicular glutamate transporters in the rat brain. J Comp Neurol. 2002; 444:39–62. [PubMed: 11835181]

Kauer JA, Malenka RC. Synaptic plasticity and addiction. Nat Rev Neurosci. 2007; 8:844–858. [PubMed: 17948030]

Kawano M, Kawasaki A, Sakata-Haga H, Fukui Y, Kawano H, Nogami H, Hisano S. Particular subpopulations of midbrain and hypothalamic dopamine neurons express vesicular glutamate transporter 2 in the rat brain. J Comp Neurol. 2006; 498:581–592. [PubMed: 16917821]

Kelley AE. Functional specificity of ventral striatal compartments in appetitive behaviors. Ann N Y Acad Sci. 1999; 877:71–90. [PubMed: 10415644]

Kritzer MF, Creutz LM. Region and sex differences in constituent dopamine neurons and immunoreactivity for intracellular estrogen and androgen receptors in mesocortical projections in rats. J Neurosci. 2008; 28:9525–9535. [PubMed: 18799684]

Le Saux M, Morissette M, Di Paolo T. ERbeta mediates the estradiol increase of D2 receptors in rat striatum and nucleus accumbens. Neuropharmacology. 2006; 50:451–457. [PubMed: 16309717]

Ledoux VA, Smejkalova T, May RM, Cooke BM, Woolley CS. Estradiol facilitates the release of neuropeptide Y to suppress hippocampus-dependent seizures. J Neurosci. 2009; 29:1457–1468. [PubMed: 19193892]

Li Y, Kolb B, Robinson TE. The location of persistent amphetamine-induced changes in the density of dendritic spines on medium spiny neurons in the nucleus accumbens and caudate-putamen. Neuropsychopharmacology. 2003; 28:1082–1085. [PubMed: 12700699]

Lynch WJ, Carroll ME. Sex differences in the acquisition of intravenously self-administered cocaine and heroin in rats. Psychopharmacology (Berl). 1999; 144:77–82. [PubMed: 10379627]

Matsuzaki M, Ellis-Davies GC, Nemoto T, Miyashita Y, Iino M, Kasai H. Dendritic spine geometry is critical for AMPA receptor expression in hippocampal CA1 pyramidal neurons. Nat Neurosci. 2001; 4:1086–1092. [PubMed: 11687814]

Matsuzaki M, Honkura N, Ellis-Davies GC, Kasai H. Structural basis of long-term potentiation in single dendritic spines. Nature. 2004; 429:761–766. [PubMed: 15190253]

Melone M, Burette A, Weinberg RJ. Light microscopic identification and immunocytochemical characterization of glutamatergic synapses in brain sections. J Comp Neurol. 2005; 492:495–509. [PubMed: 16228991]

Meredith GE. The synaptic framework for chemical signaling in nucleus accumbens. Ann N Y Acad Sci. 1999; 877:140–156. [PubMed: 10415648]

Meredith GE, Agolia R, Arts MP, Groenewegen HJ, Zahm DS. Morphological differences between projection neurons of the core and shell in the nucleus accumbens of the rat. Neuroscience. 1992; 50:149–162. [PubMed: 1383869]

Meredith GE, Pennartz CM, Groenewegen HJ. The cellular framework for chemical signalling in the nucleus accumbens. Prog Brain Res. 1993; 99:3–24. [PubMed: 7906426]

Meredith GE, Totterdell S. Microcircuits in nucleus accumbens' shell and core involved in cognition and reward. Psychobiology. 1999; 27:165–186.

Meredith GE, Ypma P, Zahm DS. Effects of dopamine depletion on the morphology of medium spiny neurons in the shell and core of the rat nucleus accumbens. J Neurosci. 1995; 15:3808–3820. [PubMed: 7751948]

Mermelstein PG. Membrane-localised oestrogen receptor alpha and beta influence neuronal activity through activation of metabotropic glutamate receptors. J Neuroendocrinol. 2009; 21:257–262. [PubMed: 19207809]

Mermelstein PG, Becker JB, Surmeier DJ. Estradiol reduces calcium currents in rat neostriatal neurons via a membrane receptor. J Neurosci. 1996; 16:595–604. [PubMed: 8551343]

Mulder AB, Hodenpijl MG, Lopes da Silva FH. Electrophysiology of the hippocampal and amygdaloid projections to the nucleus accumbens of the rat: convergence, segregation, and interaction of inputs. J Neurosci. 1998; 18:5095–5102. [PubMed: 9634575]

Ostroff LE, Fiala JC, Allwardt B, Harris KM. Polyribosomes redistribute from dendritic shafts into spines with enlarged synapses during LTP in developing rat hippocampal slices. Neuron. 2002; 35:535–545. [PubMed: 12165474]

Park M, Salgado JM, Ostroff L, Helton TD, Robinson CG, Harris KM, Ehlers MD. Plasticity-induced growth of dendritic spines by exocytic trafficking from recycling endosomes. Neuron. 2006; 52:817–830. [PubMed: 17145503]

Paxinos, G.; Watson, C. The Rat Brain in Stereotaxic Coordinates. Academic Press; New York: 1998.

Pinto A, Jankowski M, Sesack SR. Projections from the paraventricular nucleus of the thalamus to the rat prefrontal cortex and nucleus accumbens shell: ultrastructural characteristics and spatial relationships with dopamine afferents. J Comp Neurol. 2003; 459:142–155. [PubMed: 12640666]

Popov VI, Davies HA, Rogachevsky VV, Patrushev IV, Errington ML, Gabbott PL, Bliss TV, Stewart MG. Remodelling of synaptic morphology but unchanged synaptic density during late phase long-term potentiation (LTP): a serial section electron micrograph study in the dentate gyrus in the anaesthetised rat. Neuroscience. 2004; 128:251–262. [PubMed: 15350638]

Quinones-Jenab V. Why are women from Venus and men from Mars when they abuse cocaine? Brain Res. 2006; 1126:200–203. [PubMed: 17010952]

Robinson TE, Kolb B. Persistent structural modifications in nucleus accumbens and prefrontal cortex neurons produced by previous experience with amphetamine. J Neurosci. 1997; 17:8491–8497. [PubMed: 9334421]

Robinson TE, Kolb B. Alterations in the morphology of dendrites and dendritic spines in the nucleus accumbens and prefrontal cortex following repeated treatment with amphetamine or cocaine. Eur J Neurosci. 1999a; 11:1598–1604. [PubMed: 10215912]

Robinson TE, Kolb B. Morphine alters the structure of neurons in the nucleus accumbens and neocortex of rats. Synapse. 1999b; 33:160–162. [PubMed: 10400894]

Roth ME, Cosgrove KP, Carroll ME. Sex differences in the vulnerability to drug abuse: a review of preclinical studies. Neurosci Biobehav Rev. 2004; 28:533–546. [PubMed: 15527861]

Russo SJ, Festa ED, Fabian SJ, Gazi FM, Kraish M, Jenab S, Quinones-Jenab V. Gonadal hormones differentially modulate cocaine-induced conditioned place preference in male and female rats. Neuroscience. 2003; 120:523–533. [PubMed: 12890521]

Schultz KN, von Esenwein SA, Hu M, Bennett AL, Kennedy RT, Musatov S, Toran-Allerand CD, Kaplitt MG, Young LJ, Becker JB. Viral vector-mediated overexpression of estrogen receptor-alpha in striatum enhances the estradiol-induced motor activity in female rats and estradiol-modulated GABA release. J Neurosci. 2009; 29:1897–1903. [PubMed: 19211896]

Schwarz JM, Liang SL, Thompson SM, McCarthy MM. Estradiol induces hypothalamic dendritic spines by enhancing glutamate release: a mechanism for organizational sex differences. Neuron. 2008; 58:584–598. [PubMed: 18498739]

Sesack SR, Carr DB, Omelchenko N, Pinto A. Anatomical substrates for glutamate-dopamine interactions: evidence for specificity of connections and extrasynaptic actions. Ann N Y Acad Sci. 2003; 1003:36–52. [PubMed: 14684434]

Sesack SR, Pickel VM. In the rat medial nucleus accumbens, hippocampal and catecholaminergic terminals converge on spiny neurons and are in apposition to each other. Brain Res. 1990; 527:266–279. [PubMed: 1701338]

Sesack SR, Pickel VM. Prefrontal cortical efferents in the rat synapse on unlabeled neuronal targets of catecholamine terminals in the nucleus accumbens septi and on dopamine neurons in the ventral tegmental area. J Comp Neurol. 1992; 320:145–160. [PubMed: 1377716]

Shen H, Sesack SR, Toda S, Kalivas PW. Automated quantification of dendritic spine density and spine head diameter in medium spiny neurons of the nucleus accumbens. Brain Struct Funct. 2008; 213:149–157. [PubMed: 18535839]

Shi H, Cui H, Alam G, Gunning WT, Nestor A, Giovannucci D, Zhang M, Ding HF. Nestin expression defines both glial and neuronal progenitors in postnatal sympathetic ganglia. J Comp Neurol. 2008; 508:867–878. [PubMed: 18399538]

Shughrue PJ, Merchenthaler I. Distribution of estrogen receptor beta immunoreactivity in the rat central nervous system. J Comp Neurol. 2001; 436:64–81. [PubMed: 11413547]

Silverman JL, Koenig JI. Evidence for the involvement of ERbeta and RGS9-2 in 17-beta estradiol enhancement of amphetamine-induced place preference behavior. Horm Behav. 2007

Smith AD, Bolam JP. The neural network of the basal ganglia as revealed by the study of synaptic connections of identified neurones. Trends Neurosci. 1990; 13:259–265. [PubMed: 1695400]

Somogyi P, Bolam JP, Smith AD. Monosynaptic cortical input and local axon collaterals of identified striatonigral neurons. A light and electron microscopic study using the Golgi-peroxidase transport-degeneration procedure. J Comp Neurol. 1981; 195:567–584. [PubMed: 6161949]

Spruston N. Pyramidal neurons: dendritic structure and synaptic integration. Nat Rev Neurosci. 2008; 9:206–221. [PubMed: 18270515]

Swendsen J, Anthony JC, Conway KP, Degenhardt L, Dierker L, Glantz M, He J, Kalaydjian A, Kessler RC, Sampson N, Merikangas KR. Improving targets for the prevention of drug use disorders: sociodemographic predictors of transitions across drug use stages in the national comorbidity survey replication. Prev Med. 2008; 47:629–634. [PubMed: 18926848]

Thompson TL, Moss RL. Estrogen regulation of dopamine release in the nucleus accumbens: genomic- and nongenomic-mediated effects. J Neurochem. 1994; 62:1750–1756. [PubMed: 8158125]

Todtenkopf MS, Stellar JR. Assessment of tyrosine hydroxylase immunoreactive innervation in five subregions of the nucleus accumbens shell in rats treated with repeated cocaine. Synapse. 2000; 38:261–270. [PubMed: 11020229]

Totterdell S, Smith AD. Convergence of hippocampal and dopaminergic input onto identified neurons in the nucleus accumbens of the rat. J Chem Neuroanat. 1989; 2:285–298. [PubMed: 2572241]

Voorn P, Jorritsma-Byham B, Van Dijk C, Buijs RM. The dopaminergic innervation of the ventral striatum in the rat: a light- and electron-microscopical study with antibodies against dopamine. J Comp Neurol. 1986; 251:84–99. [PubMed: 3760260]

Walker QD, Rooney MB, Wightman RM, Kuhn CM. Dopamine release and uptake are greater in female than male rat striatum as measured by fast cyclic voltammetry. Neuroscience. 2000; 95:1061–1070. [PubMed: 10682713]

Woolley CS, McEwen BS. Estradiol mediates fluctuation in hippocampal synapse density during the estrous cycle in the adult rat. J Neurosci. 1992; 12:2549–2554. [PubMed: 1613547]

Zahm DS. An electron microscopic morphometric comparison of tyrosine hydroxylase immunoreactive innervation in the neostriatum and the nucleus accumbens core and shell. Brain Res. 1992; 575:341–346. [PubMed: 1349255]

Zahm DS. Functional-anatomical implications of the nucleus accumbens core and shell subterritories. Ann N Y Acad Sci. 1999; 877:113–128. [PubMed: 10415646]

Zahm DS, Brog JS. On the significance of subterritories in the “accumbens” part of the rat ventral striatum. Neuroscience. 1992; 50:751–767. [PubMed: 1448200]

Zhang D, Yang S, Yang C, Jin G, Zhen X. Estrogen regulates responses of dopamine neurons in the ventral tegmental area to cocaine. Psychopharmacology (Berl). 2008; 199:625–635. [PubMed: 18516717]

Zhou J, Nannapaneni N, Shore S. Vessicular glutamate transporters 1 and 2 are differentially associated with auditory nerve and spinal trigeminal inputs to the cochlear nucleus. J Comp Neurol. 2007; 500:777–787. [PubMed: 17154258]

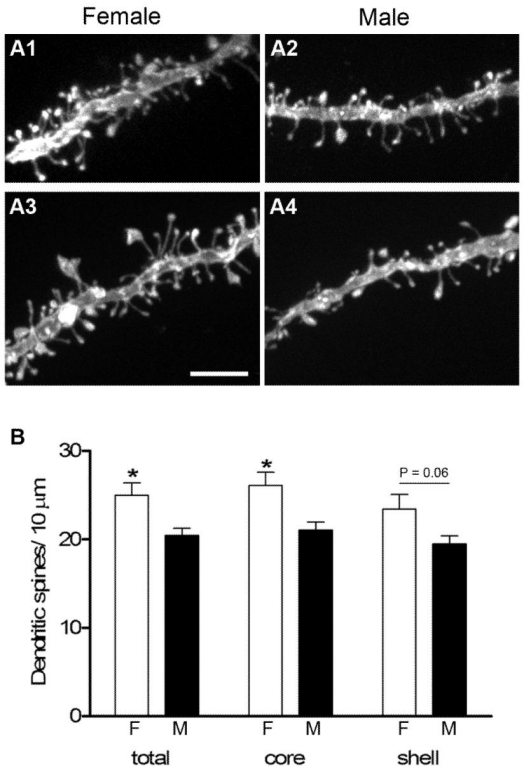

Figure 1.

A1-A4: Projected confocal images of representative DiI-labeled dendritic segments from medium spiny neurons in the core (A1, A2) and shell (A3, A4) of the NAc used for spine density measurements. **B:** Females (F) had significantly greater spine density than males (M), both in the core alone (P = 0.017) as well as in the core and shell combined (total, P = 0.017). There was a trend toward a sex difference in the shell (P = 0.06). Scale bar in A = 5 µm.

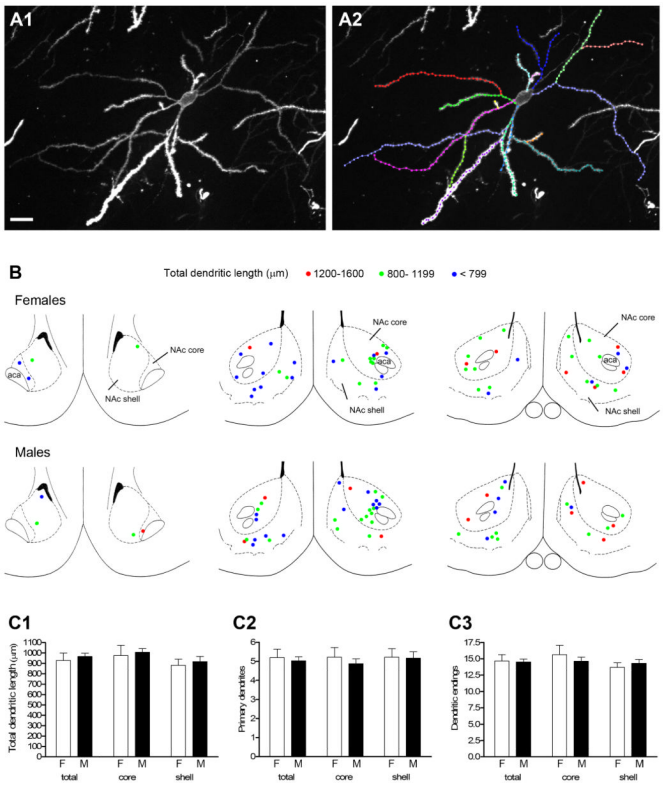

Figure 2.

A1: Projected confocal image of a DiI-labeled medium spiny neuron from the core of the NAc. **A2:** The same cell in A1 with individual dendritic branches traced and color coded for morphological analyses; this neuron had a total dendritic length of 1347 μm. **B:** Rostral to caudal (left to right) coronal sections (adapted from Paxinos and Watson, 1998) through the NAc depicting location of labeled neurons used for the whole cell analysis in males and females. Cells are represented by left and right hemisphere and color coded for total dendritic length (see key). Rostral-most section corresponds to cells imaged at approximately Bregma 2.7 mm; middle section to cells imaged from Bregma 2.2 - 1.6 mm and caudal section to cells imaged from Bregma 1.2 - 0.7 mm. **C1-C3:** No sex differences were found in any morphological measure including total dendritic length (C1), number of primary dendrites (C2), or number of dendritic endings (C3). Scale bar in A = 20 μm. Magenta-green version of panel 2B can be found as a supplementary figure.

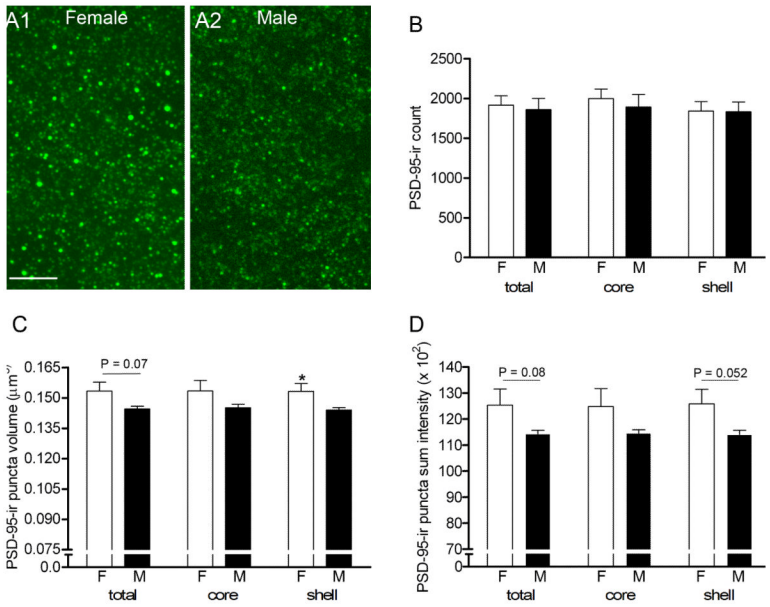

Figure 3.

A1-A2: Confocal images of PSD-95-ir puncta in the shell of a representative female (A1) and male (A2). **B:** No sex differences in the density of PSD-95-ir puncta were found in the NAc (total) or major subregions (core and shell). **C:** Mean volume of puncta was sexually dimorphic (P = 0.037) in the shell, and there was a trend toward a sex difference with the core and shell combined (P = 0.07). **D:** Mean sum intensity of puncta was higher in females but not significantly different. Scale bar in A = 5 µm.

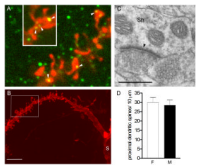

Figure 4.
A: Single optical sections (0.2μm thickness) of a DiI-labeled dendrite (red) also immunostained for PSD-95 (green). Note that PSD-95-ir puncta were found on spine heads (arrowheads) but also on the shaft of the dendrite (inset, arrowheads). **B:** A lower magnification projected confocal image of the same segment of dendrite in A (indicated by white box) to illustrate the thickness of the dendritic shaft and proximity to the soma (S). **C:** Electron micrograph illustrating an asymmetric (excitatory) synapse (arrowhead) on a dendritic shaft (Sh) in the NAc. **D:** No sex difference was found in spine density on thick, proximal dendritic segments. Scale bar in B = 5 μm; in C = 0.5 μm. Magenta-green version of panel 4A can be found as a supplementary figure.

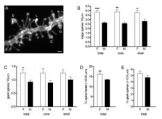

Figure 5.

A: Confocal image of a DiI-labeled dendritic segment to illustrate variation in spine head size. Spine heads ≥ 0.65 μm in diameter were classified as large (L) and those ≥ 0.9 μm in diameter were classified as giant (G). **B:** Females had a significantly greater density of large spines than males in the total NAc, and in both the core and the shell subregions (***P = 0.0003; **P = 0.001; *P = 0.01). **C:** Females had a greater density of giant spines in total NAc (*P = 0.03). **D, E:** Females had a significantly greater percentage of large (D) but not giant (E) spine heads in total NAc (core and shell combined) (**P = 0.003). Scale bar in A = 1 μm.

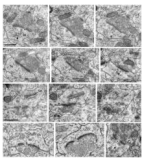

Figure 6.
Electron micrographs of giant (A-D) and large (E) spine heads in the NAc, all of which contain a perforated, asymmetric (excitatory) synapse (*). **A1-A6:** Serial sections through a giant spine head (Sp) that synapses with a bouton shared with a second, small spine (visible in A1-A4). Arrowhead in A1 indicates a clump of recycling endosomes and can also be seen in other panels. **B1-B3:** Serial sections through a giant spine head with a well defined spine apparatus (SA). **C:** A giant spine head containing a spine apparatus (SA) forms a perforated synapse (asterisk). **D:** A giant, goblet-shaped spine head encircling an excitatory bouton packed with vesicles also forms a perforated synapse (asterisk). **E:** Example of a large spine head, which forms a perforated synapse and contains a clump of recycling endosomes (arrowhead). Scale bar in A1 = 0.5 μm and applies to A1-6. Scale bar in B1 = 0.5 μm and applies to B-E.

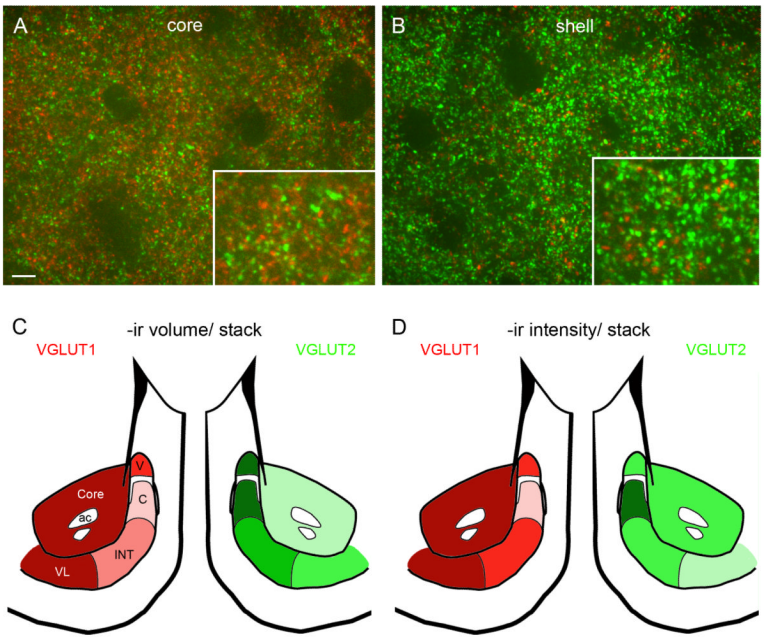

Figure 7.

A, B: Representative confocal images of the NAc core and shell illustrating double label immunofluorescence for VGLUT1 (red) and VGLUT2 (green). Boxes show higher magnification of the same image. **C, D:** Schematics showing variation in volume and intensity of VGLUT1 and VGLUT2-ir in the core and vertex (V), cone (C), intermediate (INT) and ventrolateral (VL) subregions of the NAc shell. Darker colors represent greater volume/intensity (see text for details). Note that VGLUT1: VGLUT2-ir ratio is greater in the core and ventrolateral shell while VGLUT2: VGLUT1-ir ratio is greater in the dorsomedial shell (vertex, cone and intermediate). Scale bar in A = 5 μm and applies to A and B. Magenta-green version of panels 7A-D can be found as a supplementary figure.

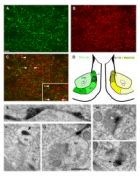

Figure 8.

A-C: Confocal image showing single channels (A and B) and overlay (C) of double-label immunofluorescence for TH-ir (green) and VGLUT2-ir (red) in the vertex subregion of the NAc shell. Arrowheads in C indicate some examples of colocalization; box in C is higher magnification of the same area. **D:** Schematics showing variation in TH-ir volume and percent volume of TH colocalized with VGLUT2 in the core and vertex (V), arch (A), cone (C), intermediate (INT) and ventrolateral (VL) subregions of the shell. Darker colors represent greater values (see text for details). An alternating pattern of high (vertex, cone, ventrolateral) and medium (arch, intermediate) levels of TH-ir is found among shell subregions; TH-ir is lowest in the core. Percentage of TH-ir volume colocalized with VGLUT2 is greatest in the dorsomedial shell (vertex, arch, cone) and lowest in the core and ventrolateral shell. **E-I:** Electron micrographs of TH-ir profiles in the NAc. **E:** A large, varicose TH-ir axon (black reaction product) along the periphery of a soma. **F, G:** Examples of TH-ir (arrowhead) adjacent to spine heads (Sp) that form asymmetric (excitatory) synapses. **H, I:** Examples of TH-ir (arrowhead) in boutons that form asymmetric synapses with spine heads; TH-ir can be proximal (H) or distal (I) to the synapse. Scale bar in A = 5 μm and applies to A-C; Scale bar in G = 0.5 μm and applies to E-I. Magenta-green version of panels 8A-C can be found as a supplementary figure.

TABLE 1

Primary antibodies used

Antigen	Immunogen	Manufacturer	Dilution used
Vesicular glutamate transporter 1 (VGLUT1)	Synthetic peptide from rat VGLUT1 protein (aa 542-560)	Chemicon/Millipore (Billerica, MA), guinea pig polyclonal, #AB5905	1:2,000
Vesicular glutamate transporter 2 (VGLUT2)	Strep-Tag® fusion protein of rat VGLUT2/DNPI (aa 510-582)	Synaptic Systems (Göttingen, Germany), rabbit polyclonal, #135402	1:1,000
Post Synaptic Density-95 (PSD-95)	Synthetic peptide from human PSD-95 (aa 310-336)	Cell Signaling (Danvers, MA), rabbit polyclonal, #2507	1:200
Tyrosine hydroxylase (TH)	Rat TH	Sigma (St. Louis, MO), mouse monoclonal, #T1299, clone TH-2	1:1000
Tyrosine hydroxylase (TH)	Denatured TH from rat pheochromocytoma	Chemicon/Millipore, rabbit polyclonal, #AB152	1:2000